RSC Advances

PAPER

View Article Online
View Journal | View Issue

Cite this: *RSC Adv.*, 2022, **12**, 15241

Dynamic reversible adhesives based on crosslinking network *via* Schiff base and Michael addition†

Junyu Ren,[a] Hongxing Yang,[a] Yingchen Wu,[a] Sichen Liu,[a] Kelu Ni,[a] Xin Ran,[a] Xiaojian Zhou,[a] Wei Gao,[a] Guanben Du*[ab] and Long Yang*[ab]

It is of practical interest to obtain polymers with complex material properties in a simplified synthetic manner for a broader range of practical applications. In this work, we constructed a dynamic reversible adhesive based on branched polyamine (PA) and *p*-formylphenyl acrylate (FPA) by simultaneously performing Michael addition reaction and Schiff base reaction. Branched polyamines provide a large number of amino groups as reaction sites that can react with both carbon–carbon double bonds and aldehyde groups. This enables the branched polymeric adhesive system to have a large number of Schiff base bonds within it, an important property of Schiff base bonds is that they are dynamically reversible. This allows us to prepare adhesives with hyperbranched crosslinking networks and recycling properties, and we have verified that FPA–PA adhesives do not exhibit significant fatigue after multiple recycling through the gluing-destruction-gluing process. The resulting FPA–PA adhesives produce tough bonding on multi-substrates such as steel, aluminum, glass, PVC, PTFE, birch and moso bamboo, which exhibited by lap shear strength of 2.4 MPa, 1.7 MPa, 1.4 MPa, 1.3 MPa, 0.4 MPa, 1.6 MPa, and 1.8 MPa, respectively. The feasibility of the synthesis idea of simultaneous Michael addition reaction and Schiff base reaction was demonstrated, as well as the excellent performance and great application potential of FPA–PA adhesives to be recyclable on multi-substrates.

Received 9th April 2022
Accepted 12th May 2022

DOI: 10.1039/d2ra02299k

rsc.li/rsc-advances

1. Introduction

Modern functional adhesives often face more complex application environments, which means that adhesives need increasingly complex properties and often require multiple functions.[1–5] Numerous researchers have developed and prepared adhesives with underwater adhesion,[6–11] multiple substrate adhesion,[12–16] stretchability,[17,18] self-healing,[19] biosustainability,[20–22] moldability,[23] *etc.* However, this not only requires a more complex structure of the polymer but also means that the conditions and steps required for synthesis become more cumbersome.[24,25] How to prepare multifunctional adhesives by a more simplified route is of greater importance for the research development of adhesive polymers.[26] Obviously, the choice of reaction substrate and the type of reaction chosen are important guidelines for the preparation of multifunctional adhesives. The preparation of multifunctional adhesives by Michael addition reaction[27–31] and Schiff base reaction[32–36] synthesis becomes an attractive solution.

Michael addition is a conjugate addition reaction through an electrophilic electron acceptor with a nucleophilic electron donor and is one of the more established classes of common methods for growing carbon chains. For example, the hyperbranched polymers with hydrophobic main chains and hydrophilic side chains prepared by Liu *et al.*[37] form cohesion by self-aggregation of hydrophobic interactions and replace water molecules on the adhering surfaces in the aqueous environment thus achieving wet adhesion. Schiff bases are formed by the condensation of amines and active carbonyl groups, which are a class of aldehydes and ketones containing carbonyl groups that undergo nucleophilic addition to amines, and have a wide range of applications in the field of adhesives. Such as, Chen *et al.*[38] enabled the rapid adhesion of hydrogels and organogels at the interface of macroscopic gel sheets to form macroscopic organic hydrogel mixtures by Schiff base bonding. Interestingly their reaction conditions are similar, which leads us to speculate that the polymers produced by the Michael addition reaction and the Schiff base reaction can be obtained in a single step.

Meanwhile, the modification of adhesive polymers by the introduction of hyperbranched polymers[39–41] has recently become a new research hotspot due to the excellent properties

[a]*International Joint Research Center for Biomass Materials, Yunnan Province Key Lab of Wood Adhesives and Glued Products, Southwest Forestry University, Kunming, 650224, China. E-mail: guanben@swfu.edu.cn; long133109070@126.com*

[b]*Key Laboratory for Forest Resources Conservation and Utilization in the Southwest Mountains, Ministry of Education, Southwest Forestry University, Kunming, 650224, China*

† Electronic supplementary information (ESI) available. See https://doi.org/10.1039/d2ra02299k

of hyperbranched polymers. Hyperbranched polymers are very different from linear polymers in terms of physicochemical properties. For example, hyperbranched polymers have a viscosity that does not change with molecular weight, are end-rich in reactive functional groups, are relatively simple to prepare, and can often be synthesized in a "one-step" process. Many studies,[42–44] including our previous work,[45] have shown that hyperbranched polymers have great potential for applications in adhesives.

In this work, we report the construction of a novel series of hyperbranched polymeric FPA–PA adhesives by a one-step method using branched polyamines PA_{4N}, PA_{5N}, and PA_{6N} as reaction substrates and *p*-formylphenyl acrylate (FPA)[46–50] with both carbon–carbon double bonds and aldehyde groups (Scheme 1). Branched polyamines obtained from the reaction of methyl acrylate with ethylenediamine, diethylenetriamine and triethylenetetramine have the advantage of being easy to prepare and having a large number of amino groups. Branched polyamines contain a large number of amino groups, which provide abundant active sites for modification, and the FPA molecules contain both carbon–carbon double bonds and aldehyde groups. The carbon–carbon double bond and the amino group can undergo Michael addition reactions, which are easy to carry out and usually do not require additional catalysts or produce additional products. Besides, the aldehyde group and the amino group can undergo Schiff base reactions rapidly. Because of the similarities in the conditions required for these two types of reactions, we can obtain FPA–PA adhesives produced from branched polyamines and FPA by Michael addition reaction and Schiff base reaction in a single step. It exhibits strong bonding performance on the glass, aluminum, steel, wood, bamboo, PTFE, and PVC substrates due to the strong cross-linked structural network established by FPA–PA adhesives through multiple interactions and the tough bonding on different substrates. At the same time, there are a large number of imine bonds in FPA–PA adhesives. Since the Schiff base reaction is an equilibrium reaction, *i.e.*, the aldehyde group and the amino group can easily remove a molecule of water to generate imine bonds, and at the same time, the imine bonds can easily absorb a molecule of water to generate the aldehyde group and the amino group again, so the imine bonds are dynamic and reversible.[51–54] The results revealed that the FPA–PA adhesives have dynamic reversible properties, and it has no fatigue in FPA–PA adhesives after cycling the gluing–destroying–gluing process 18 times. The adhesive strength did not vary much and remained at a similar level overall, indicating that FPA–PA adhesives have excellent reusability. Through Michael addition and Schiff base reactions we have prepared hyperbranched polymeric adhesives with more complex structures in a simplified route, enabling tough bonding on a wide range of substrates with dynamic reversibility and excellent bonding performance after multiple damage cycles. This study provides an important route for the preparation of multifunctional adhesives by a simplified route.

2. Experimental section

2.1. Materials

Methyl acrylate, ethylenediamine, diethylenetriamine, triethylenetetramine, acryloyl chloride, triethylamine, *p*-hydroxybenzaldehyde, methanol (MeOH), and dichloromethane (DCM) were purchased from Shanghai Adamas Reagent Co., Ltd. (Shanghai, China). All the chemicals were used without any further purification.

2.2. Characterizations methods

Differential scanning calorimetry (DSC), thermogravimetric analysis (TGA), Fourier transform infrared spectrometer (ATR-FTIR), X-ray photoelectron spectroscopy (XPS), ^{1}H NMR, and ^{13}C NMR measurements were provided in the ESI.†

2.3. Synthesis of branched polyamines PA_{4N}, PA_{5N}, and PA_{6N}

The synthesis of branched polyamines PA_{4N}, PA_{5N}, and PA_{6N} was carried out concerning the work of Yang *et al.*[45]

2.4. Synthesis and characterization of *p*-formylphenyl acrylate (FPA)

Adding *p*-hydroxybenzaldehyde (5 g, 41 mmol), triethylamine (6.5 mL), and DCM (50 mL) to a 250 mL round bottom flask,

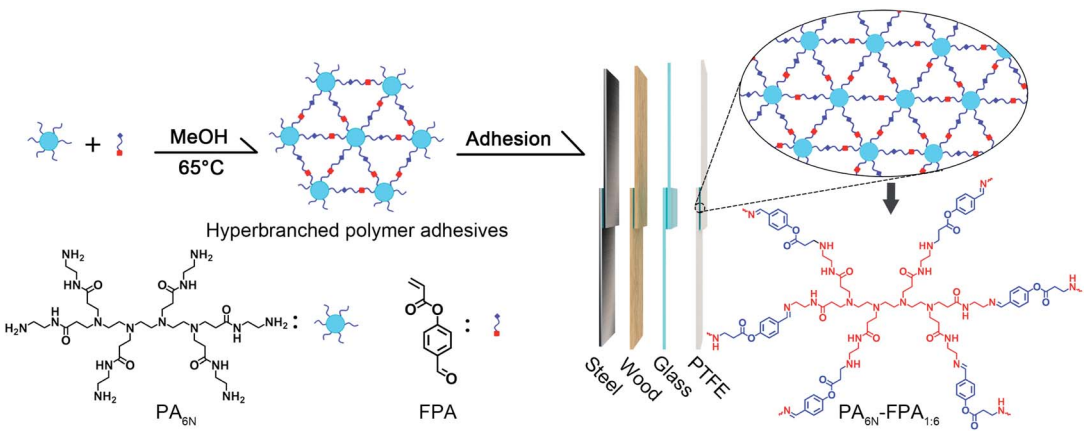

Scheme 1 Synthesis of FPA–PA branched polymeric adhesives and illustration of gluing to different substrates.

cool to 0 °C in an ice bath and stir until completely dissolved. Acryloyl chloride (4.5 g, 50 mmol) was dissolved in 10 mL of DCM and added dropwise to a round bottom flask. The reactants were then brought to room temperature overnight. After the reaction was completed, triethylamine hydrochloride was removed by filtration, extracted with saturated $NaHCO_3$, and the organic phase was dried with Na_2SO_4 and the product was collected by rotary evaporation. After purification by silica gel chromatography (PE/EA = 20/1), the product was collected by rotary evaporation and drying with a yield of about 85%. The ^1H NMR and ^{13}C NMR spectra of the FPA were obtained (Fig. S1 and S2†).

2.5. Synthesis of FPA–PA adhesives

As an example, PA_{6N}–$FPA_{1:6}$ was added to a 250 mL round bottom flask with 100 mL of methanol and PA_{6N} (10 g, 12 mmol) and stirred to allow complete dissolution. After FPA (12.7 g, 72 mmol) was completely dissolved in 50 mL of methanol, it was added dropwise to a round bottom flask and heated to reflux overnight. After the reaction, the product was collected by rotary evaporation (yield ~ 99%). The PA_{4N}–$FPA_{1:4}$, PA_{4N}–$FPA_{1:2}$, PA_{5N}–$FPA_{1:5}$, PA_{5N}–$FPA_{2:5}$, and PA_{6N}–$FPA_{1:3}$ adhesives were synthesized and prepared in the same manner as PA_{6N}–$FPA_{1:6}$ with molar ratios of 1 : 4, 1 : 2, 1 : 5, 2 : 5 and 1 : 3, respectively.

2.6. Adhesion test

Adhesion tests were all performed with glass, aluminum, steel, wood, bamboo, Teflon, and PVC substrates. All substrates are rectangular in shape 10 × 2.5 × 0.5 cm and have a hole at the end for a pin. The liquid adhesive was deposited on a 2.5 × 1.5 cm area substrate by heating and then covered with another substrate to form a substrate/adhesive/substrate sandwich structure, which was cured at room temperature for one day. We determined the thickness of the adhesive layer by vernier calipers to be about 0.5 mm ± 0.1 mm. The lap shear strength test was performed on an ETM-104B tension machine (Shenzhen Wance Testing Machine Co., Ltd). The lap shear strength test stretches the bonded joint at a displacement rate (2 mm min^{-1}) until the base material separates. After testing, the strength was calculated by dividing the lap area measured with vernier calipers by the fracture load (N). Parallel experiments were performed using six samples and the average values were calculated.

Wood-based substrate gluing properties were evaluated by using the birch and moso bamboo. The FPA–PA adhesive (80% or 100% solid content) was applied to the birch or moso bamboo substrate and then covered with another substrate to form a substrate/adhesive/substrate sandwich structure, which cured at room temperature for one day in the absence and presence of a 5 MPa pressure. Parallel experiments were performed using six samples and the average values were calculated.

Dynamic reversible cycle testing was performed using PA_{5N}–$FPA_{2:5}$ adhesive on steel and glass substrates to test the lap shear strength. The re-curing process was heated at 170 °C for 5 minutes and lap-glued again at room temperature for 30 minutes without pressure. After cooling to room temperature, the lap shear strength test was performed. Six samples were used for parallel experiments and the average value was calculated.

3. Results and discussion

3.1. DSC results analysis

The temperature has a large effect on adhesives and is an important factor in evaluating adhesive systems. For example, the temperature has different meanings for thermoset adhesives and thermoplastic adhesives. We used DSC to analyze the thermodynamic behavior of FPA–PA adhesives at a heating rate of 10 °C min^{-1}, and the results are shown in Fig. 1. The thermodynamic behavior of the six adhesives was very similar, with the heat absorption peak of PA_{4N}–$FPA_{1:4}$ at approximately 228 °C and that of PA_{4N}–$FPA_{1:2}$ at approximately 232 °C. The heat absorption peak of PA_{5N}–$FPA_{1:5}$ was at approximately 236 °C and that of PA_{5N}–$FPA_{2:5}$ at approximately 240 °C. The heat absorption peak of PA_{6N}–$FPA_{1:6}$ was at approximately 233 °C, while the peak of heat absorption of PA_{6N}–$FPA_{1:3}$ is about 235 °C. The peak of heat absorption of PA_{6N}–$FPA_{1:3}$ is about 235 °C. It can be seen that the prepared FPA–PA adhesives have the characteristics of heat absorption and melting, so FPA–PA adhesives are typical hot melt adhesives. Interestingly, the position of the heat absorption peak is lower for all systems with higher FPA content, which indicates that the thermal melting point of the hyperbranched polymer network is lower as the FPA increases in the system, implying that an increase in FPA content may suppress the cross-linking degree of the FPA–PA branched polymer network.

3.2. TGA results analysis

As shown in Fig. 2, we used a thermogravimetric analyzer (TGA) to study the thermal stability of FPA–PA adhesive. From the results, PA_{4N}–$FPA_{1:4}$, PA_{4N}–$FPA_{1:2}$, PA_{5N}–$FPA_{1:5}$, PA_{5N}–$FPA_{2:5}$, PA_{6N}–$FPA_{1:6}$, and PA_{6N}–$FPA_{1:3}$ polymers exhibited similar weight loss processes during the warming process. A very slow weight loss occurred in the temperature range of 100–200 °C. The FPA–PA adhesive exhibited very good thermal stability. The weight-loss rates of PA_{4N}–$FPA_{1:4}$, PA_{5N}–$FPA_{1:5}$, and PA_{6N}–$FPA_{1:6}$ adhesives were significantly accelerated at around 200 °C and then decreased, and increased again at around 350 °C. The PA_{4N}–$FPA_{1:2}$, PA_{5N}–$FPA_{2:5}$, and PA_{6N}–$FPA_{1:3}$ adhesives, on the other hand, reach their highest weight loss rates at about 300 °C and then level off. All FPA–PA adhesives still have approximately 20% mass remaining. Compared with PA_{4N}, PA_{5N} and PA_{6N}, the FPA–PA adhesives have better thermal stability. This is because the introduction of FPA monomer generates a cross-linked network and a large number of benzene rings form a π–π stacking structure, which gives the polymer a dense network structure and acts as a thermal barrier.

Interestingly, PA_{4N}–$FPA_{1:4}$, PA_{5N}–$FPA_{1:5}$, and PA_{6N}–$FPA_{1:6}$ had the highest weight loss rates at around 200 °C, while PA_{4N}–$FPA_{1:2}$, PA_{5N}–$FPA_{2:5}$, and PA_{6N}–$FPA_{1:3}$ had the highest weight loss rates around 300 °C. This may be because excess FPA

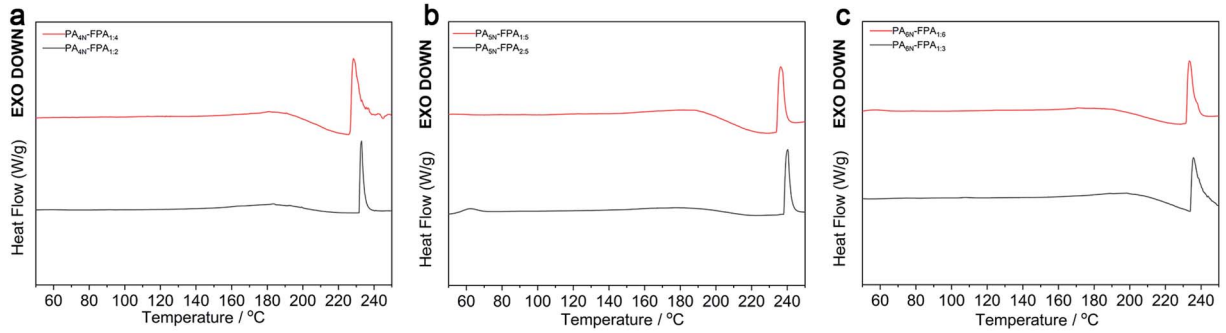

Fig. 1 (a) DSC spectra of PA_{4N}–$FPA_{1:4}$ and PA_{4N}–$FPA_{1:2}$. (b) DSC spectra of PA_{5N}–$FPA_{1:5}$ and PA_{5N}–$FPA_{2:5}$. (c) DSC spectra of PA_{6N}–$FPA_{1:6}$ and PA_{6N}–$FPA_{1:3}$.

occupies more amino sites in the polymer network, making the excess carbon–carbon double bonds as well as aldehyde groups unable to continue the reaction thus reducing the cross-linking degree of the cross-linked network. This means that the introduction of more FPA does not better improve the thermal stability of the polymer and may suppress the degree of cross-linking of the hyperbranched polymer network, which is also consistent with the DSC results.

3.3. ATR-FTIR results analysis

Fig. 3 shows the attenuated total reflectance (ATR) FTIR spectra of PA_{4N}–$FPA_{1:4}$, PA_{4N}–$FPA_{1:2}$, PA_{4N}, PA_{5N}–$FPA_{1:5}$, PA_{5N}–$FPA_{2:5}$, PA_{5N}, PA_{6N}–$FPA_{1:6}$, PA_{6N}–$FPA_{1:3}$, and PA_{6N}. This reflects the consumption status of FPA during the reaction with polyamines. The characteristic ATR-FTIR peaks observed in the branched polymers, including ν(N–H) located at 3274 cm^{-1}, and δ (N–H) located at 1551 cm^{-1} (amide II bands), which is attributed to the abundance of amide bonds in the polymer. The characteristic peaks ν(C–H) located at 2828 and 2943 cm^{-1} represent the methylene CH_2 on the branched chain of the polymer. Compared with the ATR-FTIR spectra of PA_{4N}, PA_{5N}, and PA_{6N}, the ATR-FTIR spectra of FPA–PA adhesives appeared with new characteristic peaks at 839 cm^{-1} and 1160 cm^{-1}, which are ascribed to γ(=C–H) of the out-of-plane bending

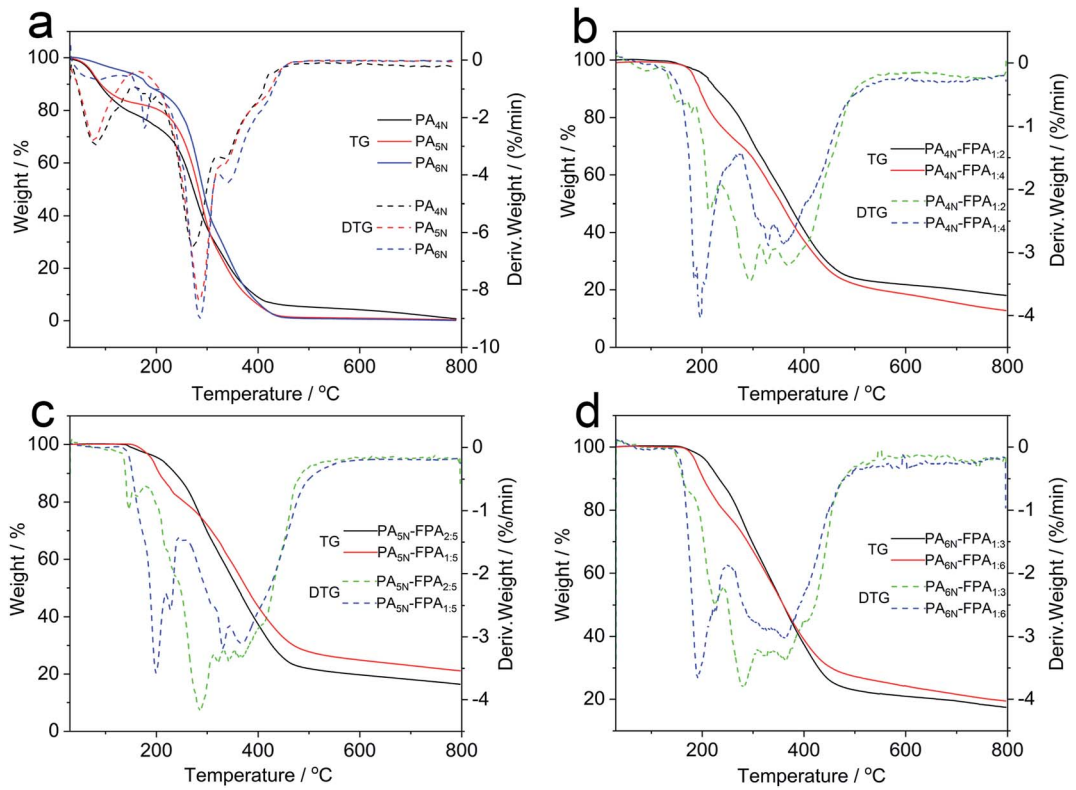

Fig. 2 (a) Thermogravimetric spectra of PA_{4N}, PA_{5N} and PA_{6N}. (b) Thermogravimetric spectra of PA_{4N}–$FPA_{1:4}$ and PA_{4N}–$FPA_{1:2}$. (c) Thermogravimetric spectra of PA_{5N}–$FPA_{1:5}$ and PA_{5N}–$FPA_{2:5}$. (d) Thermogravimetric spectra of PA_{6N}–$FPA_{1:6}$ and PA_{6N}–$FPA_{1:3}$.

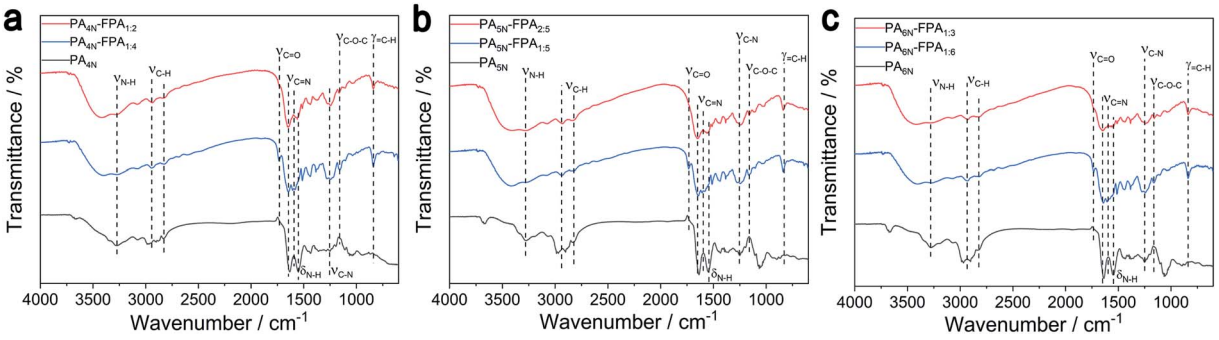

Fig. 3 (a) ATR-FTIR spectra of PA_{4N}–$FPA_{1:4}$, PA_{4N}–$FPA_{1:2}$ and PA_{4N}. (b) ATR-FTIR spectra of PA_{5N}–$FPA_{1:5}$, PA_{5N}–$FPA_{2:5}$ and PA_{5N}. (c) ATR-FTIR spectra of PA_{6N}–$FPA_{1:6}$, PA_{6N}–$FPA_{1:3}$ and PA_{6N}.

vibration (*para*-substitution) of the benzene ring structure and ν(C–O) of the ester group, respectively. This indicates the successful introduction of FPA in FPA–PA adhesives. Compared to PA_{4N}, PA_{5N}, and PA_{6N}, new characteristic peaks can be seen at about 1644 cm^{-1} in the ATR-FTIR spectra of FPA–PA adhesives, which is the characteristic peak of the ν(C=N) imine bond formed by the reaction of the amino and aldehyde groups. We observed a new aldehyde group characteristic peak of the ν(C=O) at 1735 cm^{-1} for PA_{4N}–$FPA_{1:4}$, PA_{5N}–$FPA_{1:5}$, and PA_{6N}–$FPA_{1:6}$, which was absent from PA_{4N}–$FPA_{1:2}$, PA_{5N}–$FPA_{2:5}$, and PA_{6N}–$FPA_{1:3}$. This is due to the excess of FPA in PA_{4N}–$FPA_{1:4}$, PA_{5N}–$FPA_{1:5}$, and PA_{6N}–$FPA_{1:6}$, where the aldehyde group is not completely consumed. Also, a more pronounced peak appears at 1250 cm^{-1}, which is due to the addition reaction of carbon–carbon double bonds and amino groups to produce more ν(C–N). This preliminarily confirmed that the carbon–carbon double bond in FPA had a Michael addition reaction with the amino group in PA, and the formation of the imine bond also proved that the aldehyde group in FPA had a Schiff base reaction with the amino group in PA.

3.4. XPS results analysis

We further investigated the chemical composition and structure of FPA–PA adhesives using XPS. The PA_{4N}–$FPA_{1:2}$ adhesive showed C, N, O signals in XPS spectra as shown in Fig. 4a, where the C, N, and O atomic contents of PA_{4N}–$FPA_{1:2}$ were 73.79%, 16.86%, and 9.35%, respectively. As shown in Fig. 4b, the C 1s spectrum of PA_{4N}–$FPA_{1:2}$ has five peaks at 284.8 eV, 285.6 eV, 286.6 eV, 287.6 eV, and 288.7 eV, corresponding to the C–C, C–N, C=N, C=O and O–C=O groups, respectively.[55] The N 1s spectrum of PA_{4N}–$FPA_{1:2}$ (Fig. 4c) has three peaks at 398.9 eV, 399.9 eV, and 401.2 eV, which are attributed to N=C, N–C, and N–H groups, respectively.[45] The O 1s spectrum of PA_{4N}–$FPA_{1:2}$ (Fig. 4d) has two peaks at 531.1 eV and 532.3 eV, attributed to the C=O and C–O groups, respectively.[39] It can be found that the C=N group can be observed in the C 1s spectrum, and the C=N group can be observed in the N 1s spectrum. The results indicate that the Schiff base reaction occurred with the smooth formation of imine bonds between FPA and branched polyamines. The XPS spectra results of the PA_{4N}–$FPA_{1:4}$ adhesive (Fig. S3†) was similar to those of PA_{4N}–$FPA_{1:2}$.

3.5. NMR analysis of the adhesive

We further determined by ^{1}H NMR spectrum whether there are excess carbon–carbon double bonds and aldehyde groups remaining in the polymer (Fig. 5, S4–S9†). We can see a distinct aldehyde group characteristic peak at about 10 ppm and a distinct carbon–carbon double bond characteristic peak at 6.0–6.7 ppm in the ^{1}H NMR spectrum of FPA (Fig. S1†). In contrast, in the ^{1}H NMR spectrum of PA_{4N}–$FPA_{1:4}$, PA_{4N}–$FPA_{1:2}$, PA_{5N}–$FPA_{1:5}$, PA_{5N}–$FPA_{2:5}$, PA_{6N}–$FPA_{1:6}$ and PA_{6N}–$FPA_{1:3}$, we did not observe the characteristic peaks of carbon–carbon double bonds at 6.0–6.7 ppm. In Fig. S5, S7, and S9,† we can observe the obvious characteristic peak of the aldehyde group at 9.7–10 ppm, which is absent in Fig. S4, S6, and S8.† This indicates that the carbon–carbon double bonds and aldehyde groups of FPA are almost completely consumed in PA_{4N}–$FPA_{1:2}$, PA_{5N}–$FPA_{2:5}$, and PA_{6N}–$FPA_{1:3}$. In PA_{4N}–$FPA_{1:4}$, PA_{5N}–$FPA_{1:5}$, and PA_{6N}–$FPA_{1:6}$, the carbon–carbon double bond of FPA is almost completely consumed and the aldehyde group remains. The amino group undergoes more addition reactions with the carbon–carbon double bond during the reaction, resulting in some aldehyde groups not being able to participate in the reaction and forming capped ends. The degree of cross-linking of PA_{4N}–$FPA_{1:4}$, PA_{5N}–$FPA_{1:5}$ and PA_{6N}–$FPA_{1:6}$ adhesives with excess FPA was reduced, which is consistent with the results of DSC and TG.

3.6. Analysis of the adhesion performance of different substrates

The adhesion of FPA–PA adhesives to a wide range of substrate surfaces is a distinctive feature. We tested the adhesion performance of FPA–PA adhesives by using various types of typical substrates such as steel, aluminum, glass, PVC, and PTFE. And the results are shown in Fig. 6a (Table S1†). From the results, it is known that FPA–PA adhesives have a tough adhesion on steel, aluminum, glass, PVC, and PTFE substrates. The introduction of FPA constructed a highly cross-linked polymer network structure *via* Schiff base and Michael addition reactions. Multiple groups in the polymer enable multiple interactions between the branched polymer and the substrate, resulting in high lap shear strength (Fig. 6b). For example, functional groups such as benzene rings, ester groups, and

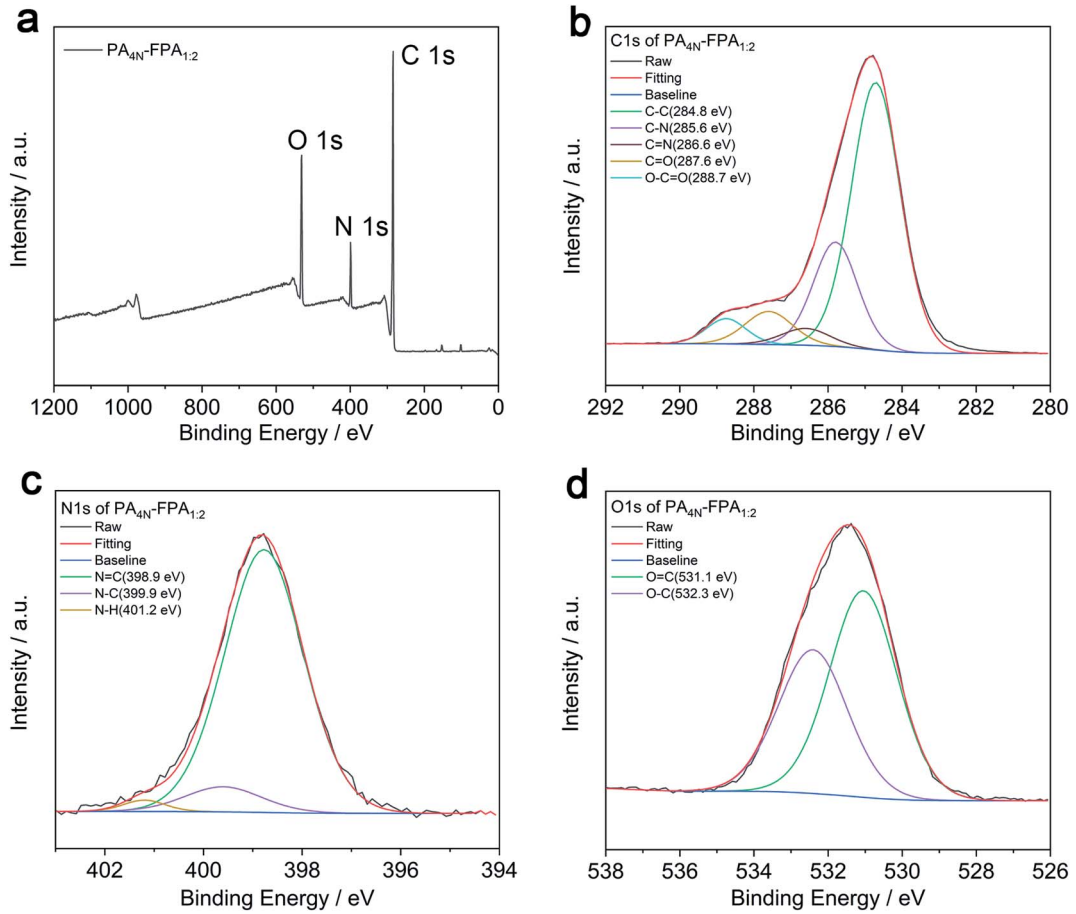

Fig. 4 (a) XPS measurement spectra of PA_{4N}–$FPA_{1:2}$. (b) C 1s high-resolution spectrum of PA_{4N}–$FPA_{1:2}$. (c) N 1s high-resolution spectrum of PA_{4N}–$FPA_{1:2}$. (d) O 1s high-resolution spectrum of PA_{4N}–$FPA_{1:2}$.

aldehyde groups can form interactions such as hydrogen bonds, electrostatic interactions, and metal chelating with the substrate.[1] Compared to FPA unsaturated adhesives, FPA saturated adhesives such as PA_{4N}–$FPA_{1:4}$ achieve higher adhesion strength on steel and glass substrates. The NMR and FTIR results show that FPA saturated adhesives contain more aldehyde residues, which allows a large number of aldehyde groups to chelate with the steel surface and form more hydrogen bonds on the glass surface. Therefore, higher adhesion strength is achieved compared to FPA unsaturated adhesives. On PVC substrate, the FPA–PA adhesive crosses the interface with the substrate, spreading and twisting around each other to produce adhesion strength. The hydrogen atoms of the amino group can form coordination bonds with the surface of the PTFE substrate, resulting in strong bonding strength. It is the ability of FPA–PA adhesives to interact with a wide range of substrates in various covalent and non-covalent ways that gives FPA–PA adhesives their strong bonding strength on different substrate surfaces.[1,45]

At the same time, we tested the glue stability and adhesion performance of FPA–PA adhesive soaked in water (Fig. S10†). FPA unsaturated adhesives such as PA_{5N}–$FPA_{2:5}$ completely lost bond strength after 24 h, while FPA saturated adhesives such as PA_{5N}–$FPA_{1:5}$ lost strength completely after 48 h. Obviously, the increase in the amount of FPA enhances the water-resistance of the adhesive. This is because a large number of hydrophobic structures in FPA, such as the large stacking of ester groups and benzene rings, form a barrier and prolong the time required for hydrolysis. It shows the possibility of improving water-resistance by introducing hydrophobic groups and provides ideas for further modification.

3.7. Analysis of wood substrate adhesion properties

We have investigated the adhesion performance of FPA–PA adhesives on wood materials using birch and moso bamboo as substrates. In Fig. 7a, FPA–PA adhesive (80% solid content) was used and cured at room temperature for 1 day. In Fig. 7b, FPA–PA adhesive (100% solid content) was used and cured at room temperature for 1 day. In Fig. 7c, FPA–PA adhesive (100% solid content) was used and cured for 1 day at room temperature under 5 MPa pressure. The FPA–PA adhesive (80% solid content) contains a 20% mass fraction of methanol present. Compared to FPA–PA adhesive (100% solid content), it has a certain degree of fluidity at room temperature and is easier to apply.

In the results of Fig. 7a, there is a tendency to increase the adhesion strength of FPA–PA adhesives with increasing number of terminal amino groups. This may be due to the higher degree

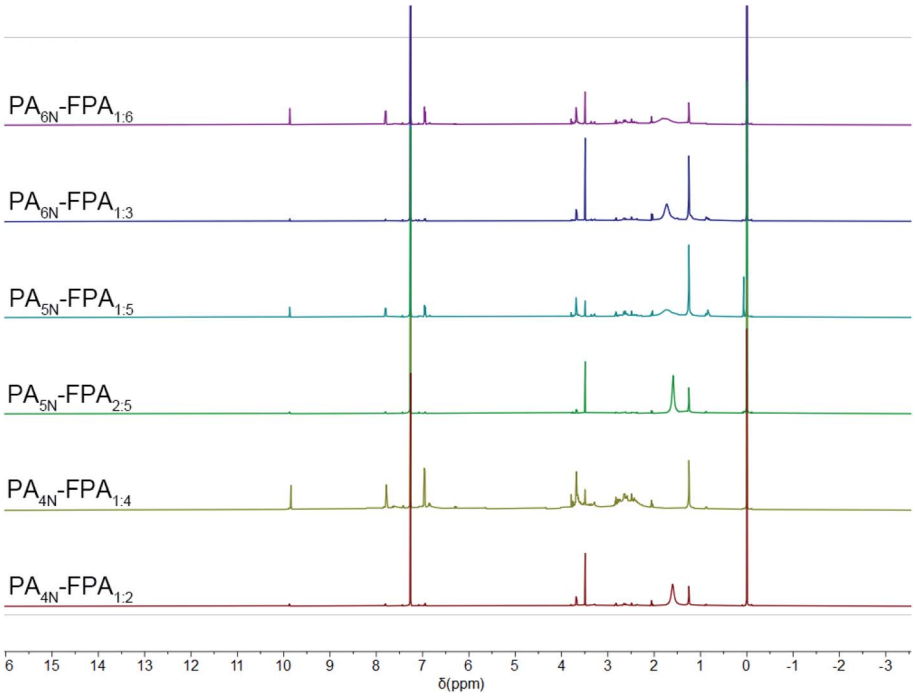

Fig. 5 ^{1}H NMR spectrum (600 MHz, $CDCl_3$, rt) of PA_{4N}–$FPA_{1:4}$, PA_{4N}–$FPA_{1:2}$, PA_{5N}–$FPA_{1:5}$, PA_{5N}–$FPA_{2:5}$, PA_{6N}–$FPA_{1:6}$, and PA_{6N}–$FPA_{1:3}$.

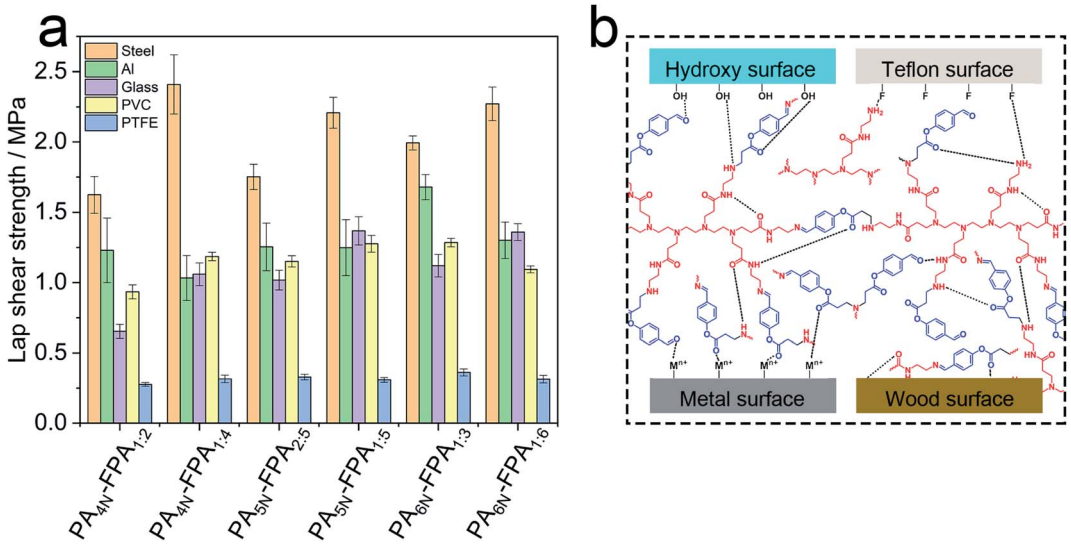

Fig. 6 (a) Schematic diagram of the tensile shear strength of FPA–PA adhesives on steel, aluminum, glass, PVC, and PTFE. (b) Schematic diagram of the bonding strength generated by FPA adhesives and different substrates, such as hydrogen bonding, metal chelation, ligand bonding and mechanical mosaic.

of branched crosslinking in the crosslinking network structure of FPA–PA adhesives as the number of terminal amino groups increases. Compared to moso bamboo substrate, birch substrate has a rougher surface and more pores. Since FPA–PA adhesive (80% solid content) has better flow ability, it can able to interact sufficiently with rough birch wood substrate to form mechanical mosaic, and the bonding strength is higher than in moso bamboo substrate. However, the results in Fig. 7b demonstrate the trend of decreasing adhesion strength of FPA–PA adhesives (100% solid content) on wood substrates with the number of terminal amino groups and the degree of crosslinking. This is probably because the FPA–PA adhesive (100% solid content) loss of good flowability, making it difficult for the adhesive to interact sufficiently with the substrate. The rough, porous birch substrate has less actual contact with the adhesive, so its adhesion strength is lower on birch substrates than on moso bamboo substrate. Moreover, PA_{4N}–$FPA_{1:4}$, PA_{5N}–$FPA_{1:5}$ and PA_{6N}–$FPA_{1:6}$ adhesives (80% solid content and 100% solid

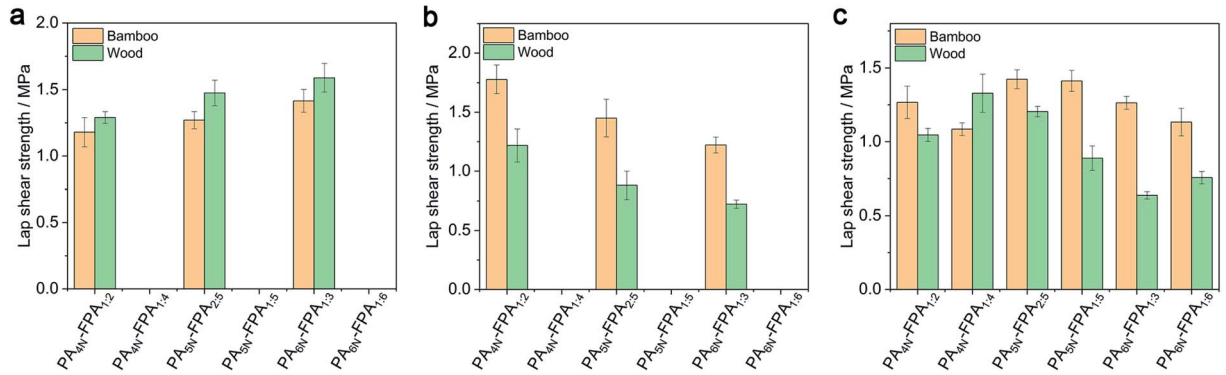

Fig. 7 (a) Tensile shear strength of adhesive with 80% solid content on wood substrate. (b) Tensile shear strength of 100% solid content adhesive on wood substrate. (c) Tensile shear strength of 100% solid content adhesive on the wood substrate by applying 5 MPa pressure.

content) failed to finish curing after one day of curing at room temperature. This is due to the fact that the degree of cross-linking of the polymer is reduced due to the excess of FPA, so the curing process becomes more difficult. When the curing time is extended, it is also able to finish curing on wood and bamboo substrates. This shows that FPA–PA adhesives can be cured on steel, aluminum, glass, PVC, PTFE, wood, and bamboo, but the requirements for curing time are different, which is also due to the different surface groups and surface energies (Table S2 and S3†) of different substrates. In the results of Fig. 7c, using FPA–PA adhesives (100% solid content) and applying 5 MPa pressure, we found that the PA_{4N}–$FPA_{1:4}$, PA_{5N}–$FPA_{1:5}$ and PA_{6N}–$FPA_{1:6}$ adhesives were also fully cured. Without pressure, we measured the thickness of the adhesive layer to be 0.5 mm ± 0.1 mm, while the thickness of the pressed adhesive layer was 0.3 mm ± 0.1 mm. This also proves that the contact between the adhesive layer and the substrate will be much closer. This indicates that the adhesive layer and the substrate are in closer contact due to pressure, forcing a tighter bond between the adhesive and the substrate to facilitate the curing of the adhesive.

3.8. Dynamic reversible cycle test analysis

We tested the lap shear strength by using PA_{5N}–$FPA_{2:5}$ adhesive on steel and glass substrates and then heated the separated substrates and the residual adhesive to bond them again. The lap shear strength was tested after curing at room temperature for 30 minutes, and the results of repeating the previous operation are shown in Fig. 8a. We can see that PA_{5N}–$FPA_{2:5}$ adhesive has no fatigue phenomenon after many cycles, and the strength of 18 cycles does not change much, which indicates its good reusability. And we analyzed the variation in storage modulus (G') and loss modulus (G'') of PA_{5N}–$FPA_{2:5}$ adhesive over a temperature range of 80 °C to 140 °C, and the heating rate of 5 °C min^{-1} (Fig. 8b). Both G'' and G' increased when the temperature decreased from 140 °C to 90 °C, and G'' started to override G' at 99 °C, which means that curing behavior occurred. At the same time, the variation of storage modulus (G') and loss modulus (G'') was studied for strains from 0.01 to 1000 (%) at 160 °C (Fig. S11†).

Clearly, the G' and G'' values of the adhesive increase rapidly with decreasing temperature, with a clear intersection at

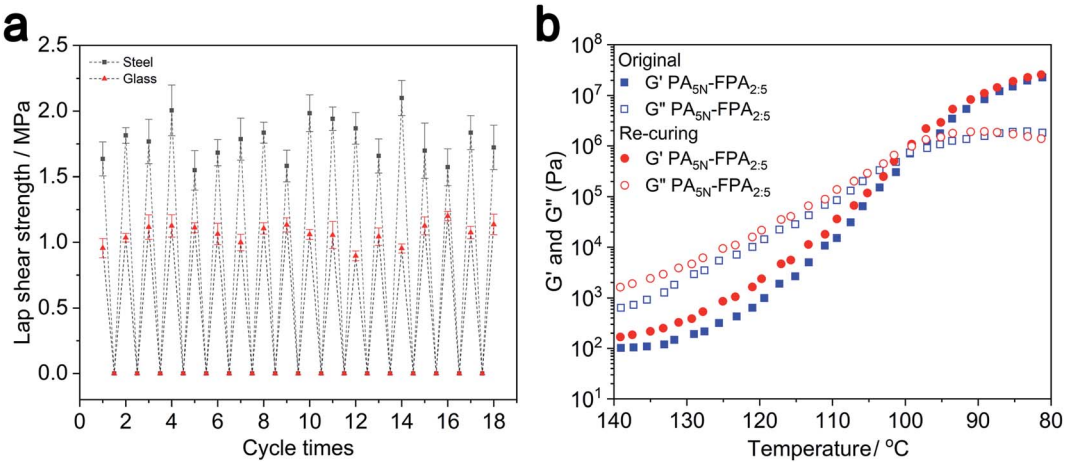

Fig. 8 (a) Schematic diagram of the strength of PA_{5N}–$FPA_{2:5}$ glued–destroyed–glued cycles on steel and glass substrates. (b) Temperature-dependent variation in G' and G'' of PA_{5N}–$FPA_{2:5}$ adhesive.

approximately 99 °C. The G' and G'' values decrease rapidly with increasing temperature, implying owing to the dynamic breakage of noncovalent interactions in polymer networks, such as hydrogen bonds and Schiff base bonds. As the temperature decreased, the noncovalent interactions in the polymer network recovered again such that the G' and G'' values rose rapidly and eventually recovered almost completely. As the strain increases from 0.01% to 100%, the G' and G'' values of the adhesive remain almost constant. Even when very high strains of $\gamma =$ 1000% were applied to induce fracture or detrimental damage to the adhesive, efficient healing was observed after the adhesive was allowed to relax back to low strain. This is due to the fact that even though a large number of dynamic bonds have been broken at high temperatures, the polymer itself still has an entangled network structure. When the strain is too high, the disruption of chain-to-chain entanglement and friction leads to a rapid decrease in G' and G''. When the strain decreases, it is clear that the degree of entanglement between the chains is not fully recovered, and the values of G' and G'' are recovered by about half. At the same time at 80 °C, we see that the G' and G'' of the adhesive can reach 2.57×10^7 Pa and 1.8×10^6 Pa, respectively, which are much higher than the values of G' and G'' at 160 °C. This indicates that the main source of the mechanical strength of the adhesive is the noncovalent interactions force that exists abundantly in the cross-linked network structure. This makes FPA–PA adhesives have strong reusability and have important application value.

4. Conclusions

In this study, we constructed a new kind of FPA–PA adhesives by using branched polyamines (PA_{4N}, PA_{5N}, and PA_{6N}) to react with FPA monomers by performing Michael addition reactions and Schiff base reactions. The ability to bond on a wide range of substrates such as steel, aluminum, glass, PVC, PTFE, birch, and moso bamboo is due to the complex and diverse functional groups in FPA–PA adhesives that provide a variety of covalent and non-covalent bonding forces. Interestingly, the Michael addition reaction and the Schiff base reaction can occur simultaneously under the same conditions, allowing the final synthetic preparation to be obtained in a single reaction, which has obvious advantages in terms of industrial production. The bonding performance of various substrates and FPA–PA adhesives with different solid contents were studied. The results show that FPA–PA adhesives have a good bonding effect on steel, aluminum, glass, PVC, and PTFE substrates. Due to enough imine bonds present in its structure, the FPA–PA adhesives exhibited excellent recyclability, which has no fatigue after 18 cycles of gluing–destroying–gluing on glass and steel substrates. It demonstrates the excellent performance and great application potential of FPA–PA adhesives for recyclability on a wide range of substrates.

Conflicts of interest

There are no conflicts to declare.

Acknowledgements

This work was financially supported by Applied Basic Research Program of Yunnan Province (No. 202001AW070017, 202101AT070047), National Natural Science Foundation of China (No. 32171884, 32060323, 32071688), and the Key Project of National Natural Science Foundation of China (No. 30930074). G. D. acknowledges Program for Leading Talents, Department of Science and Technology of Yunnan Province (No. 2017HA013). L. Y. acknowledges Candidates of the Young and Middle-Aged Academic Leaders of Yunnan Province (202105AC160048), the Ten Thousand Talent Program for Young Top-notch Talents of Yunnan Province (YNWR-QNBJ-2020-136), the National Post-Doctoral Innovative Talent Support Program of China (No. BX20190291), and the 111 project (D21027).

References

1 C. Cui, R. Gu, T. Wu, Z. Yuan, C. Fan, Y. Yao, Z. Xu, B. Liu, J. Huang and W. Liu, *Adv. Funct. Mater.*, 2022, **32**, 2109144.
2 B. D. B. Tiu, P. Delparastan, M. R. Ney, M. Gerst and P. B. Messersmith, *ACS Appl. Mater. Interfaces*, 2019, **11**, 28296–28306.
3 Z. Wang, S. Zhang, S. Zhao, H. Kang, Z. Wang, C. Xia, Y. Yu and J. Li, *Chem. Eng. J.*, 2021, **404**, 127069.
4 Z. Wang, S. Zhao, R. Song, W. Zhang, S. Zhang and J. Li, *Sci. Rep.*, 2017, **7**, 1–10.
5 X. Li, J. Lai, Y. Deng, J. Song, G. Zhao and S. Dong, *J. Am. Chem. Soc.*, 2020, **142**, 21522–21529.
6 Y. Zhou, C. Zhang, S. Gao, W. Li, J.-j. Kai and Z. Wang, *ACS Appl. Mater. Interfaces*, 2021, **13**, 50451–50460.
7 M. Dompé, F. J. Cedano-Serrano, M. Vahdati, L. van Westerveld, D. Hourdet, C. Creton, J. van der Gucht, T. Kodger and M. Kamperman, *Adv. Mater. Interfaces*, 2020, **7**, 1901785.
8 Y. Wang, V. Kang, W. Federle, E. Arzt and R. Hensel, *Adv. Mater. Interfaces*, 2020, **7**, 2001269.
9 M. Zhao, L. Bai and J. Jang, *Appl. Surf. Sci.*, 2020, **511**, 145589.
10 C. Liang, Z. Ye, B. Xue, L. Zeng, W. Wu, C. Zhong, Y. Cao, B. Hu and P. B. Messersmith, *ACS Appl. Mater. Interfaces*, 2018, **10**, 25017–25025.
11 H. Y. Yuen, H. P. Bei and X. Zhao, *Chem. Eng. J.*, 2021, **431**, 133372.
12 Z.-H. Liu, J.-Q. Huang, L.-J. Sun, D. Lei, J. Cao, S. Chen, W.-C. Shih, F.-L. Qing and Z.-W. You, *Chinese. J. Polym. Sci.*, 2018, **36**, 58–64.
13 J. Zhu, X. Lu, W. Zhang and X. Liu, *Macromol. Rapid Commun.*, 2020, **41**, 2000098.
14 H. M. Siebert and J. J. Wilker, *ACS Sustain. Chem. Eng.*, 2019, **7**, 13315–13323.
15 G. Schmidt, K. H. Smith, L. J. Miles, C. K. Gettelfinger, J. A. Hawthorne, E. C. Fruzyna and J. J. Wilker, *Adv. Sust. Syst.*, 2022, 2100392.
16 B. D. James, K. M. Kimmins, M.-T. Nguyen, A. J. Lausch and E. D. Sone, *Sci. Rep.*, 2021, **11**, 1–10.

17 R. Zhang, H. Peng, T. Zhou, Y. Yao, X. Zhu, B. Bi, X. Zhang, B. Liu, L. Niu and W. Wang, *ACS Appl. Polym. Mater.*, 2019, **1**, 2883–2889.
18 D. Gan, W. Xing, L. Jiang, J. Fang, C. Zhao, F. Ren, L. Fang, K. Wang and X. Lu, *Nat. Commun.*, 2019, **10**, 1–10.
19 S. Song, H. Yang, Y. Cui, Y. Tang, Y. Chen, B. Yang, J. Yuan and J. Huang, *Polymer*, 2020, **198**, 122528.
20 S. Zhao, Z. Wang, Z. Li, L. Li, J. Li and S. Zhang, *ACS Appl. Mater. Interfaces*, 2019, **11**, 32414–32422.
21 H. Pang, Q. Yan, C. Ma, S. Zhang and Z. Gao, *ACS Appl. Mater. Interfaces*, 2021, **13**, 59527–59537.
22 Z. Tang, M. Zhang, H. Xiao, K. Liu, X. Li, B. Du, L. Huang, L. Chen and H. Wu, *ACS Biomater. Sci. Eng.*, 2022, **8**, 1096–1102.
23 H. Cho, G. Wu, J. C. Jolly, N. Fortoul, Z. He, Y. Gao, A. Jagota and S. Yang, *Proc. Natl. Acad. Sci. U.S.A.*, 2019, **116**, 13774–13779.
24 Y. Okaya, Y. Jochi, T. Seki, K. Satoh, M. Kamigaito, T. Hoshino, T. Nakatani, S. Fujinami, M. Takata and Y. Takeoka, *Macromolecules*, 2019, **53**, 374–386.
25 G. P. Maier, M. V. Rapp, J. H. Waite, J. N. Israelachvili and A. Butler, *Science*, 2015, **349**, 628–632.
26 Q. Zhang, C.-Y. Shi, D.-H. Qu, Y.-T. Long, B. L. Feringa and H. Tian, *Sci. Adv.*, 2018, **4**, eaat8192.
27 S. Omura, Y. Kawazoe and D. Uemura, *Materials*, 2021, **14**, 5479.
28 A. Rather, N. Jana, S. Begum, H. Srivastava and U. Manna, *Green Chem.*, 2017, **19**, 4527–4532.
29 Z. Zeng, X.-m. Mo, C. He, Y. Morsi, H. El-Hamshary and M. El-Newehy, *J. Mater. Chem. B*, 2016, **4**, 5585–5592.
30 B. D. Mather, K. Viswanathan, K. M. Miller and T. E. Long, *Prog. Polym. Sci.*, 2006, **31**, 487–531.
31 T. Xie, J. Ding, X. Han, H. Jia, Y. Yang, S. Liang, W. Wang, W. Liu and W. Wang, *Mater. Horiz.*, 2020, **7**, 605–614.
32 Y. Wu, L. Yuan, N.-a. Sheng, Z.-q. Gu, W.-h. Feng, H.-y. Yin, Y. Morsi and X.-m. Mo, *Front. Mater. Sci.*, 2017, **11**, 215–222.
33 J. Liu, J. Li, F. Yu, Y.-x. Zhao, X.-m. Mo and J.-f. Pan, *Int. J. Biol. Macromol.*, 2020, **147**, 653–666.
34 X. Gong, Z. Cheng, S. Gao, D. Zhang, Y. Ma, J. Wang, C. Wang and F. Chu, *Carbohydr. Polym.*, 2020, **250**, 116846.
35 J. Pang, S. Bi, T. Kong, X. Luo, Z. Zhou, K. Qiu, L. Huang, X. Chen and M. Kong, *Carbohydr. Polym.*, 2020, **237**, 116138.
36 H. Guo, S. Huang, A. Xu and W. Xue, *Chem. Mater.*, 2022, **34**, 2655–2671.
37 C. Cui, C. Fan, Y. Wu, M. Xiao, T. Wu, D. Zhang, X. Chen, B. Liu, Z. Xu and B. Qu, *Adv. Mater.*, 2019, **31**, 1905761.
38 G. Deng, Q. Ma, H. Yu, Y. Zhang, Z. Yan, F. Liu, C. Liu, H. Jiang and Y. Chen, *ACS Macro Lett.*, 2015, **4**, 467–471.
39 S. Liu, G. Du, H. Yang, H. Su, X. Ran, J. Li, L. Zhang, W. Gao and L. Yang, *ACS Sustain. Chem. Eng.*, 2021, **9**, 16849–16861.
40 T. Li, B. Zhang, S. Jiang, X. Zhou, G. Du, Z. Wu, M. Cao and L. Yang, *ACS Sustain. Chem. Eng.*, 2020, **8**, 5209–5216.
41 S. Liang, Y. Zhang, H. Wang, Z. Xu, J. Chen, R. Bao, B. Tan, Y. Cui, G. Fan and W. Wang, *Adv. Mater.*, 2018, **30**, 1704235.
42 Y. Tang, C. K. Jim, Y. Liu, L. Ye, A. Qin, J. W. Lam, C. Zhao and B. Z. Tang, *ACS Appl. Mater. Interfaces*, 2010, **2**, 566–574.
43 R. Mezzenga, L. Boogh and J.-A. E. Månson, *Compos. Sci. Technol.*, 2001, **61**, 787–795.
44 D. Lu, Y. Zhang, Y. Li, H. Wang, Z. Shen, Q. Wei and Z. Lei, *Polym. Chem.*, 2016, **7**, 1963–1970.
45 H. Yang, G. Du, Z. Li, X. Ran, X. Zhou, T. Li, W. Gao, J. Li, H. Lei and L. Yang, *ACS Appl. Polym. Mater.*, 2021, **3**, 1638–1651.
46 E. Subramanyam, S. Mohandoss and H. W. Shin, *J. Appl. Polym. Sci.*, 2009, **112**, 2741–2749.
47 D. Xu, Z. Cao, T. Wang, J. Zhong, J. Zhao, F. Gao, X. Luo, Z. Fang, J. Cao and S. Xu, *Prog. Org. Coat.*, 2019, **135**, 510–516.
48 Y. Wang, H. Yu, H. Yang, X. Hao, Q. Tang and X. Zhang, *Macromol. Chem. Phys.*, 2017, **218**, 1700348.
49 J. Salaklang, V. Maes, M. Conradi, R. Dams and T. Junkers, *React. Chem. Eng.*, 2018, **3**, 41–47.
50 F. Xin, Y. Li, C. Fu, I. Javed, X. Huang, A. Schaschkow, R. S. Garcia Ribeiro, E. N. Gurzov, T. P. Davis and X. Zhang, *Chem. Mater.*, 2020, **32**, 1080–1088.
51 C. D. Meyer, C. S. Joiner and J. F. Stoddart, *Chem. Soc. Rev.*, 2007, **36**, 1705–1723.
52 M. E. Belowich and J. F. Stoddart, *Chem. Soc. Rev.*, 2012, **41**, 2003–2024.
53 A. Chao, I. Negulescu and D. Zhang, *Macromolecules*, 2016, **49**, 6277–6284.
54 H. Zhang, D. Wang, W. Liu, P. Li, J. Liu, C. Liu, J. Zhang, N. Zhao and J. Xu, *J. Polym. Sci., Part A: Polym. Chem.*, 2017, **55**, 2011–2018.
55 X. Ran, Q. Qu, X. Qian, W. Xie, S. Li, L. Li and L. Yang, *Sens. Actuators, B*, 2018, **257**, 362–371.